Unstable dimension variability and synchronization of chaotic systems

Ricardo L. Viana[1] and Celso Grebogi[2]
[1]*Departamento de Física, Universidade Federal do Paraná, 81531-990, Curitiba, PR, Brazil*
[2]*Department of Mathematics, Institute for Plasma Research and Institute for Physical Science and Technology, University of Maryland, College Park, Maryland 20742*
(Received 27 September 1999; revised manuscript received 29 March 2000)

The nonhyperbolic structure of synchronization dynamics is investigated in this work. We argue analytically and confirm numerically that the chaotic dynamics on the synchronization manifold exhibits an unstable dimension variability, which is an extreme form of nonhyperbolicity. We analyze the dynamics in the synchronization manifold and in its transversal direction, where a tonguelike structure is formed, through a system of two coupled chaotic maps. The unstable dimension variability is revealed in the statistical distribution of the finite-time transversal Lyapunov exponent, having both negative and positive values. We also point out that unstable dimension variability is a cause of severe modeling difficulty.

PACS number(s): 05.45.Xt, 05.45.Pq

I. INTRODUCTION

We often classify dynamical systems into deterministic and stochastic ones. Deterministic systems are characterized by a set of prescribed mathematical rules which evolve the dynamical variables in time. For these kinds of models we can numerically generate trajectories over reasonably long periods of time. Stochastic systems are based on some sort of random process. They may occur when extrinsic noise is present. For these systems, only statistical information can be extracted, like averages or fluctuations of physical quantities, over trajectories of reasonable length.

In this paper we consider a new example of a third kind of dynamical system (*pseudodeterministic*), which—in spite of being deterministic—yields only statistical relevant information over trajectories of reasonable length. The problem with those systems is not related to the correctness and exactitude of the dynamical equations, but rather to a mathematical pathology called *unstable dimension variability* [1,2].

Unstable dimension variability was introduced by Abraham and Smale through a two-dimensional continuously differentiable map [3]. A feature associated with unstable dimension variability is the oscillating behavior of a finite-time Lyapunov exponent about zero. This occurs because typical trajectories present arbitrarily long (but finite-time) segments for which the orbit on the average is repelling in one of the dimensions, and other segments for which it is attracting in the same dimension. This behavior was found in a four-dimensional invertible map describing a kicked double rotor [4].

Recently a noninvertible two-dimensional map was proposed as a simple dynamical system exhibiting unstable dimension variability [2]. Moreover, it has been shown [5] that a lattice of diffusively coupled Hénon maps presents unstable dimension variability for any nonzero coupling strength. In this paper, we argue that unstable dimension variability occurs in the context of synchronization of chaotic orbits of two similar maps with nonlinear coupling. By changing variables such that one of them is in the synchronization manifold of the coupled system and the other is transversal to it, we obtain a map that was first studied in the context of superpersistent chaotic transients and crises [6]. We identify the mechanism that brings unstable dimension variability to the chaotic invariant set of this system, namely, a saddle-repeller bifurcation which was formerly related to the boundary crisis mechanism [7]. It produces a structure composed of supernarrow tongues through which trajectories on a chaotic saddle may escape after very long transients before they are reinjected. A chaotic saddle is an invariant compact set $\mathcal{C}$ that is both attracting and repelling, and contains a chaotic trajectory which is dense in $\mathcal{C}$. This structure is similar to that observed in the context of the so-called riddling bifurcations [8]. The fluctuating behavior of the transversal finite-time Lyapunov exponent is described for this example, and statistical information about its distribution is presented.

The goodness of deterministic models is determined by two well-known paradigms: (i) the model must be based on sound theoretical framework, e.g., correctly applied physical laws; and (ii) the trajectories produced by the model should reproduce correctly, in some sense, the actual behavior observed in Nature. This motivated the introduction of the *model shadowability* concept [1,5]: let A and B be two closely related dynamical models of a physical system, but with some difference, which could be related to a small change in one of the system parameter values, or a slightly different external influence on each model, or a different noise realization. The latter cause is restricted to arbitrarily small time dependent and bounded perturbations, which excludes Gaussian white noise, for example.

We say that model shadowability occurs if trajectories of model A stay close to trajectories of model B. This is necessary, but not sufficient, for either model to reproduce and predict correctly the time evolution of the system which the model is intended to describe. In other words, if there is no model shadowability neither A or B would generate trajectories that are physically realized, since if no trajectory of A is close to any trajectory of B, it is unlikely that either model would give a trajectory that stays close to any real trajectory produced by Nature.

The difficulties that obstruct model shadowability have been divided into three classes: minor, moderate, and severe

[5,9]. Minor modeling difficulties occur for hyperbolic chaotic systems, since they present sensitive dependence on initial conditions. If A and B are hyperbolic chaotic systems, trajectories of A can always be closely followed, or shadowed, by trajectories of B for an infinite time [10]. A chaotic set is hyperbolic if, at each point of a trajectory on this set, the local phase space can be split into unstable and stable subspaces, and the angle between them is bounded away from zero. The unstable (stable) subspace evolves into the unstable (stable) one along the trajectory. However, chaotic nonhyperbolic systems are much more common in physical applications—they may present nonhyperbolic (homoclinic) tangencies of the unstable and stable subspaces. For these systems we say there is a moderate modeling difficulty because trajectories of A are shadowed by trajectories of B for a long, yet finite, amount of time [11]. However, if this shadowability time is long enough, both models are still useful for describing the physical phenomena being modeled.

Finally, pseudodeterministic models present severe modeling difficulties, since they are chaotic nonhyperbolic systems presenting unstable dimension variability: the unstable and stable subspaces along a chaotic invariant set have no tangencies, but the dimension of the unstable subspace varies from point to point. For this case the shadowability time is short, and no useful information could be extracted from single trajectories over a reasonable time span, but rather statistical information based on a probability distribution [1].

This paper is organized as follows: in Sec. II we introduce the coupled chaotic map system, and analyze its synchronization manifold and the corresponding noninvertible map on a torus. Sections III and IV are devoted to a description of the saddle-repeller bifurcation, the average transient lifetime, and the birth of unstable-dimension variability. Section V deals with the distribution of finite-time transversal Lyapunov exponent and the relative fraction of its positive values. Section VI contains our conclusions.

II. COUPLED CHAOTIC MAPS

Coupled dynamical systems are susceptible to the synchronization of their trajectories, by which they undergo closely related motions, even when they are chaotic. In the latter case, even if two identical systems are started with different initial conditions, if the coupling is strong enough their states are asymptotically equal as the time evolves [12]. This is a quite different behavior, compared to that expected from uncoupled yet identical chaotic systems, since if they are started with approximately equal but different initial conditions, sensitive dependence will cause the two systems to have completely uncorrelated motion after some time [13].

We consider two piecewise maps of the form $x_{n+1}=kx_n \pmod 1$, where $k>1$. For almost all trajectories of each map the (infinite time) Lyapunov exponent $\lambda=\ln k$ is positive. By *almost all* we mean that all orbits generated from this map are chaotic, except for a set of zero Lebesgue measure containing countably infinite periodic points [13]. We can write $k=1+\alpha/2$, which is greater than one provided $\alpha>0$, and change the variable range from $[0,1)$ to $[0,2\pi)$, without altering the chaotic nature of the map orbits.

Let us introduce a nonlinear coupling of two such chaotic maps, yielding a nonlinear coupled system on a torus T^2:

$$u_{n+1}=\left(1+\frac{\alpha}{2}\right)u_n+\mathcal{U}(u_n,w_n) \pmod{2\pi}, \tag{1}$$

$$w_{n+1}=\left(1+\frac{\alpha}{2}\right)w_n+\mathcal{W}(u_n,w_n) \pmod{2\pi}, \tag{2}$$

where $\mathcal{U}$ and $\mathcal{W}$ are given by

$$\mathcal{U}(u_n,w_n)=\left(1-\frac{\alpha}{2}\right)w_n+\frac{1}{2}(u_n-w_n)^2+\frac{\beta}{2}\cos(u_n+w_n), \tag{3}$$

$$\mathcal{W}(u_n,w_n)=\left(1-\frac{\alpha}{2}\right)u_n-\frac{1}{2}(u_n-w_n)^2-\frac{\beta}{2}\cos(u_n+w_n), \tag{4}$$

where $\beta>0$.

For coupled dynamical systems like this one, we can obtain the synchronization state, which is given by $u_n=w_n$. Geometrically, this state defines a synchronization manifold $\mathcal{S}$, which is a one-dimensional subset of the phase space $T^2=[0,2\pi)\times[0,2\pi)$. If we represent this torus on a square with periodic boundaries, the synchronization manifold is a straight line with unitary slope. In order to describe the dynamics in the synchronization manifold and in the direction transversal to it, we make a coordinate transformation $\theta=u+w$, $z=u-w$. There results a two-dimensional noninvertible map on a torus:

$$\theta_{n+1}=2\theta_n \pmod{2\pi}, \tag{5}$$

$$z_{n+1}=\alpha z_n+z_n^2+\beta\cos\theta_n \quad (-2\pi<z\leqslant+2\pi). \tag{6}$$

Here the synchronization manifold $\mathcal{S}$ is simply the axis $z=0$. If $\beta=0$, the system decouples into two independent maps in θ and z, so that an initial condition in the synchronization manifold will generate a chaotic orbit $\{\theta_n\}_{n=0}^{\infty}$ with $z_n=0$ for all times—it will never escape from $\mathcal{S}$. Hence $\mathcal{S}$ is an invariant manifold only for $\beta=0$. An invariant manifold is typically related to the existence of some kind of symmetry in the system, so we may call β a *symmetry-breaking* parameter. For nonzero β, a chaotic orbit of the system is not restricted to the synchronization manifold, and can occupy a larger portion of the phase space along the transversal direction z.

The system in Eqs. (5) and (6) was introduced, in a slightly different form [6], to describe a kind of crises characterized by long-lived, or superpersistent, chaotic transients. The z part of the system was allowed to have any real value in $(-\infty,+\infty)$. For some parameter values, like $\alpha=0.7$ and $\beta=0.02$, that system, like ours given by Eqs. (5) and (6), exhibited a chaotic attractor near the $z=0$ line (Fig. 1). A crude argument that can be used to justify the chaotic nature of this attractor consists on linearizing the map in Eq. (6) about $z=0$, setting $z=\beta\zeta$, where ζ is a small quantity. We obtain the map $\zeta_{n+1}=\alpha\zeta_n+\cos\theta_n$, that would give a chaotic attractor for $|\alpha|<1$, as proved by Kaplan and Yorke [14]. In addition to this chaotic attractor, it was shown [6] that there is another chaotic set which is a chaotic saddle (a nonattracting chaotic invariant set) located where the fractal basin boundary is.

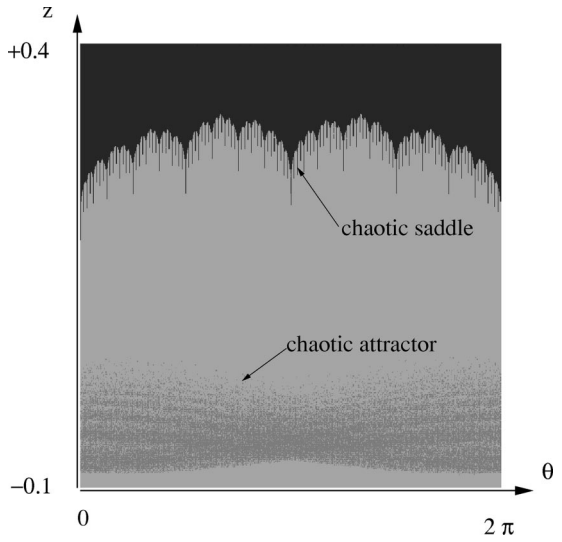

FIG. 1. Phase portrait of the map [Eqs. (5) and (6)] for $\alpha=0.7$ and $\beta=0.02<\beta_*=0.0225$. The dark region contains points which are driven to higher z values, but are eventually reinjected to negative z values due to the z dynamics being in $[-2\pi,+2\pi)$. The chaotic saddle is the boundary between the dark and light gray region. The chaotic attractor is embedded in the light gray region.

III. SADDLE-REPELLER BIFURCATION

The mechanism whereby the chaotic attractor of the map in Eqs. (5) and (6) loses hyperbolicity through unstable dimension variability is basically an unstable-unstable pair bifurcation. As a result, the chaotic attractor may collide with the chaotic saddle, and disappear into a larger chaotic saddle from which trajectories may escape, through a complex structure of supernarrow tongues. This is also called saddle-repeller bifurcation [7], and it has been found to be the cause of other strange behavior in chaotic systems, like riddling of basins of attraction [8] and boundary crises [6].

A linear stability analysis can show the basic features of this transition. The period-1 fixed points of the map of Eqs. (5) and (6) are

$$\overline{\theta}=0, \quad \overline{z}=\tfrac{1}{2}\,(1-\alpha\pm\sqrt{(1-\alpha)^2-4\beta}). \tag{7}$$

Defining $z_*=(1-\alpha)/2$ and $\beta_*=z_*^2$, these fixed points are written as $(\theta=0,\ z_b=z_*+\sqrt{\beta_*-\beta})$ and $(\theta=0,\ z_c=z_*-\sqrt{\beta_*-\beta})$. Let us fix our attention to the case depicted in Fig. 1, i.e., $\alpha=0.7$ and $\beta=0.02<\beta_*=0.0225$. It turns out that z_c lies in the upper point (i.e., the point with the highest value of z) of the chaotic attractor, whereas z_b is in the lowest point of the chaotic saddle.

The Jacobian matrix of the map has eigenvalues given by $\xi_1=2$ and $\xi_2=\alpha+2z_n$. So the θ direction is always unstable, as it should be due to the existence of the chaotic attractor. The eigenvalue related to the transversal direction, evaluated at the fixed points, gives

$$\xi_2(z_{b,c})=1\pm 2\sqrt{\beta_*-\beta}, \tag{8}$$

so that, for $\beta<\beta_*$, z_b is a repeller, since it has an unstable dimension of dimension 2, and no stable subspace at all. z_c is a saddle point, since both stable and unstable subspaces have dimensions equal to 1 [Fig. 2(a)]. If $\beta=\beta_*$ the fixed points

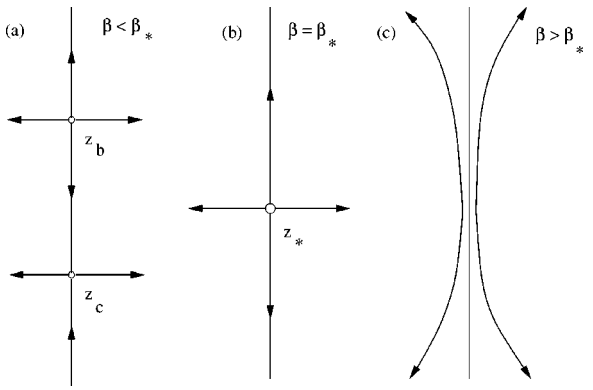

FIG. 2. Fixed points for the map [Eqs. (5) and (6)] and their stability for (a) $\beta<\beta_*$, (b) $\beta=\beta_*$, and (c) $\beta>\beta_*$.

z_c and z_b coalesce at $z=z_*$ [Fig. 2(b)]. Since the eigenvalue is equal to 1 at this point, linear stability analysis fails to determine its stability, and we have a saddle-repeller bifurcation with eigenvalue $+1$ at $\beta=\beta_*$. For $\beta>\beta_*$ the fixed points no longer exist, and we have a different dynamical behavior [Fig. 2(c)].

When the fixed points coalesce at $\beta=\beta_*$, the chaotic attractor collides with the chaotic saddle, and it becomes a *chaotic transient* through a boundary crisis (since the attractor has collided with an unstable periodic orbit) [7]. Trajectories arising from initial conditions belonging to the former basin of the chaotic attractor will typically approach its remnant, that is now a part of a larger chaotic saddle, and will bounce around it in an irregular fashion. However, after some (typically very long) time this trajectory will stay near the region where the fixed points have coalesced, and will leave the chaotic saddle, being eventually reinjected to the vicinity of the saddle due to the z dynamics being in $[-2\pi,+2\pi]$.

At the location where the fixed points coalesced $(z=z_*)$, a tongue opens up, allowing the trajectories near the chaotic saddle to escape for $\beta>\beta_*$. Simultaneously, each preimage of z_* also develops a tongue. Since these preimages are dense in the chaotic saddle, an infinite number of these tongues opens up simultaneously when $\beta=\beta_*$. Actually, these tongues will develop at those points where $\theta=2\pi m/2^k$, with m and k positive integers. For our map, however, these tongues are very narrow, since their widths decrease geometrically, and are extremely difficult to find numerically, with exception of the main tongue opened up at z_*.

IV. BEHAVIOR OF CHAOTIC TRANSIENTS

To understand how chaotic transients are formed after the saddle-repeller bifurcation, let us consider the z part of the map of Eq. (6) at $\theta=0$ (from where the main tongue grows up),

$$z_{n+1}=\alpha z_n+z_n^2+\beta, \tag{9}$$

whose fixed points z_b and z_c are the intersections between the parabolic function and the first bisector $z_{n+1}=z_n$ [Fig. 3(a)]. As β approaches its critical value β_*, these points approach each other and eventually coalesce when $\beta=\beta_*$ at

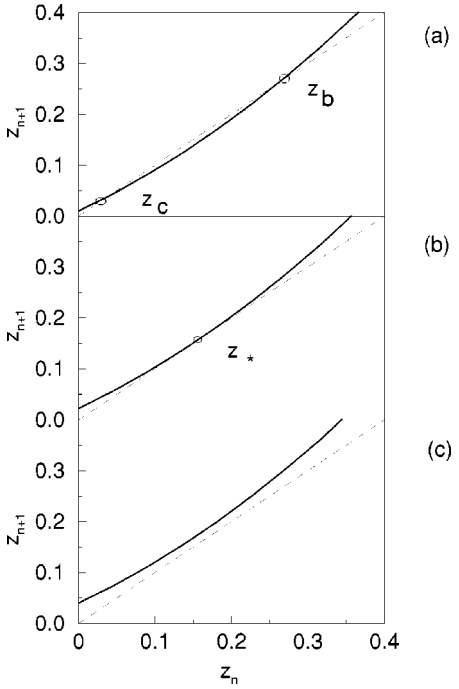

FIG. 3. First return map for Eq. (6) with $\theta=0$ and $\alpha=0.7$ for (a) $\beta=0.01<\beta_*=0.0225$, (b) $\beta=\beta_*=0.0225$, and (c) $\beta=0.04>\beta_*$.

$z=z_*$, where the map function is tangent to the 45° line [Fig. 3(b)]. For $\beta>\beta_*$ the parabola has moved upward, and does not intercept the bisector, leaving no fixed points. However, provided β is not very far from β_*, a narrow channel forms between the parabola and the 45° line, through which passes the trajectory resulting from the map iterations, staying there a very long time, and eventually escaping to large z values [Fig. 3(c)]. Because z is in a torus, map iterates are reinjected and enter again in the channel. This is the basic mechanism of type-I Intermittency [15], but since the θ direction is unstable, the slow motion through the channel does not imply a laminar behavior. Rather, it is related to a chaotic transient, that is characterized by an irregular wandering of the trajectory over a limited θ range.

The chaotic transient decays when the trajectory enters a tongue, escaping toward larger z values, before it is reinjected. The main tongue is formed about the $\theta=0$ line, so let us focus our attention at this spot. For β values greater than β_*, a tongue intercepts the synchronization manifold $z=0$ in an aperture of width l near $\theta=0$, through which the trajectory can escape. Once having entered the aperture, the trajectory stays in it a number T of iterates before leaving the region $y\leqslant y_c$. Although y_c must be less than 2π, its exact value does not affect our results in a significant way. From now on, we set $y_c=2.0$. The trajectory, however, does not immediately stays close to $\theta=0$, since the θ direction is highly unstable (its eigenvalue is $\xi_2=2>1$, pulling back the trajectory into the vicinity of the chaotic saddle).

Let l be the distance between the orbit and $\theta=0$ at a given time. After T iterates this distance increases to $(\xi_2)^T l$. However, since the θ excursion is bounded, we expect that $(\xi_2)^T l<\kappa_1$, where κ_1 is an $O(1)$ constant. Now we consider what happens with a large number of trajectories arising from randomly chosen initial conditions. Due to the ergodicity of the θ motion, we expect that almost any initial condition θ_0 will generate an orbit which has a uniform distribution over $[0,2\pi)$ for large times. Hence the probability of θ_{n+1} falling into the aperture $[-l/2,+l/2]$, if θ_n is not in this interval, is equal to the interval width l. So we can estimate the average lifetime $\langle\tau\rangle$ of the chaotic transient as the inverse of this probability. Taking our previous estimate as an upper bound for the distance along θ direction at time T, we have [7]

$$\langle\tau\rangle=\kappa(\xi_2)^T=\kappa 2^T, \tag{10}$$

where $\kappa=1/\kappa_1$.

In order to compute T, we assume that, for β slightly greater than β_* the aperture width l is very small, so that we may approximate θ by 0 and use Eq. (9) again. The difference $z_{n+1}-z_n$ has a local minimum at z_*, so we describe the dynamics within the narrow channel by using $\delta_n=z_n-z_*$. This difference evolves with time according to the map

$$\delta_{n+1}=\delta_n+\delta_n^2+(\beta-\beta_*), \tag{11}$$

and, since δ_{n+1} is very close to δ_n, we can approximate the difference $\delta_{n+1}-\delta_n$ as a differential and write a differential equation for δ, now a continuous function of time τ,

$$\frac{d\delta}{d\tau}=\delta^2+(\beta-\beta_*), \tag{12}$$

which can be integrated from -2π to $+2\pi$, to give an estimate for the time T it takes for the trajectory to escape once it has fallen in the aperture:

$$T=\frac{2}{\sqrt{\beta-\beta_*}}\arctan\left(\frac{2\pi}{\sqrt{\beta-\beta_*}}\right). \tag{13}$$

Inserting Eq. (13) into Eq. (10), and taking logarithms, we have

$$\log_{10}\langle\tau\rangle=\log_{10}\kappa+2\log_{10}2(\beta-\beta_*)^{-1/2}\times\arctan(2\pi(\beta-\beta_*)^{-1/2}). \tag{14}$$

To check the validity of the hypotheses made in the above derivation, we have made a numerical experiment, choosing N_{θ_0} initial conditions randomly distributed over $[0,2\pi)$, and computing the transient exit time once a given trajectory crosses the line $y=y_c=2.0$. The average transient lifetime $\langle\tau\rangle$ was then computed for many values of the difference $(\beta-\beta_*)^{-1/2}$, the results being depicted in Fig. 4, where the parameter κ in the theoretical prediction above is a fitting parameter.

The fitting is asymptotic though, since numerical results are best fitted by Eq. (14) when we approach β_*, i.e., in the neighborhood of the saddle-repeller bifurcation. The lifetime of the transients can be very large, for instance up to 10^8 transients, even though we are as far from β_* as 44%. This occurs because the trajectory has to stay many iterations in the narrow aperture of width l. Therefore, a better agreement between the theoretical prediction (14) and the numerical result only occurs for β closer to β_*. Far from β_*, the

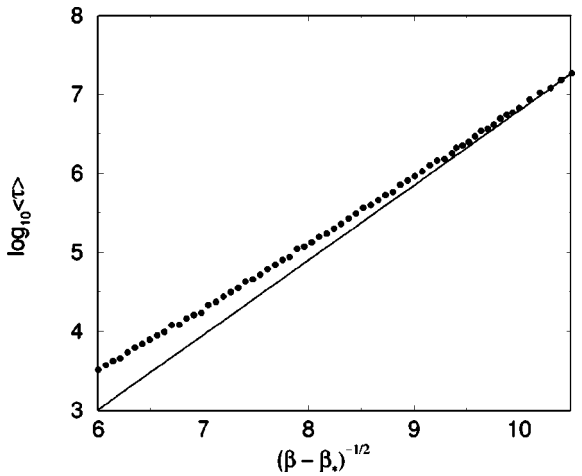

FIG. 4. Base-10 logarithm of the average exit time of transients $\langle\tau\rangle$ of the map [Eqs. (5) and (6)] with $\alpha=0.7$ and $\beta_*=0.0225$, as a function of $(\beta-\beta_*)^{-1/2}$. Circles: numerical experiment; full line: theoretical prediction given by Eq. (14) with a fitting parameter $\kappa=0.0027$.

theoretical estimate we made ceases to be valid, but remains useful as a lower bound for the exit time of transients.

V. FINITE-TIME LYAPUNOV EXPONENTS

We have seen that, at the saddle-repeller bifurcation $\beta=\beta_*$, an infinite number of points, dense on the chaotic attractor, become repellers (unstable dimension 2), and an infinite number of supernarrow tongues crop up as result of the collision between the attractor and the chaotic saddle. However, there remains a dense set of saddle points (unstable dimension one) in the invariant set, and since these two different sets are densely intertwined, unstable dimension variability does occur in the chaotic invariant set for a large range of parameter values of the map.

Yet, another signature of unstable dimension variability, as stated in Sec. I, is the fluctuating behavior of the finite-time Lyapunov exponents about zero. Consider a d-dimensional map $\mathbf{x}\mapsto\mathbf{f}(\mathbf{x})$, where $\mathbf{x}$ is a d-dimensional vector and $\mathbf{f}$ is a d-dimensional vector field. Let n be a positive integer, and let $\mathbf{Df}^n(\mathbf{x}_0)$ denote the Jacobian matrix of $\mathbf{f}^n$ (the n-times iterated map function) evaluated at the point $\mathbf{x}_0$. The eigenvalues of the Jacobian matrix $\mathbf{Df}^n(\mathbf{x}_0)$ are

$$\sigma_1(\mathbf{x}_0,n)\geqslant\sigma_2(\mathbf{x}_0,n)\geqslant\cdots\geqslant\sigma_d(\mathbf{x}_0,n)\geqslant 0. \tag{15}$$

We define the kth time-n Lyapunov exponent associated with the initial condition $\mathbf{x}_0$ as [2]

$$\lambda_k(\mathbf{x}_0,n)=\frac{1}{n}\ln\left\|\mathbf{Df}^n(\mathbf{x}_0)\mathbf{u}_k\right\|, \tag{16}$$

where $\mathbf{u}_k$ is the eigenvector corresponding to the eigenvalue σ_k. Note that the usual infinite-time Lyapunov exponent

$$\lambda_k=\lim_{n\to\infty}\lambda_k(\mathbf{x}_0,n) \tag{17}$$

has the same value for almost every initial point $\mathbf{x}_0$ with respect to the Lebesgue measure in the basin of attraction.

For our map on a two-torus, $\mathbf{x}_n=(\theta_n,z_n)^T$, the Jacobian matrix of the n-times iterated map has eigenvalues $\sigma_1=(\xi_1)^n=2^n$, and

$$\sigma_2=\prod_{i=1}^{n}(\alpha+2z_i), \tag{18}$$

so that the second (transverse) finite-time Lyapunov exponent is given by

$$\lambda_2(\mathbf{x}_0,n)=\frac{1}{n}\sum_{i=1}^{n}\ln|\alpha+2z_i|, \tag{19}$$

the first exponent being simply $\ln 2$.

The possibility of fluctuations between positive and negative values for this exponent makes it useful to define a distribution function for it. Let $P(\lambda_2(\mathbf{x}_0,n),n)$ denote the probability density function of the second time-n Lyapunov exponent, when $\mathbf{x}_0$ is chosen at random according to the Lebesgue measure. In other words, $P(\lambda_2(\mathbf{x}_0,n),n)d\lambda_2$ is the probability that the exponent value lies between λ_2 and $\lambda_2+d\lambda_2$. If $F(\lambda_2)$ is any function of the time-n Lyapunov exponent, its average over the invariant measure of the attractor is given by

$$\langle F(\lambda_2(\mathbf{x}_0,n))\rangle=\int_{-\infty}^{+\infty}F(\lambda_2(\mathbf{x}_0,n))P(\lambda_2(\mathbf{x}_0,n),n)d\lambda_2. \tag{20}$$

To obtain the distribution $P(\lambda_2)$ numerically, we picked up many randomly chosen initial conditions uniformly distributed over $[0,2\pi)$, and iterate each initial condition $\mathbf{x}_0$ a large number of times. Every $n=10$ steps we compute the time-10 exponent according to Eq. (19). Actually, we use the recurrency of dynamics, and follow a single trajectory a large number of steps, say two million iterates. The time $n=10$ exponents are then computed from 2×10^5 consecutive and nonoverlapping length-10 sections of the trajectory. From these exponents we compute a frequency histogram with convenient normalization, so that

$$\int_{-\infty}^{+\infty}P(\lambda_2(\mathbf{x}_0,n),n)d\lambda_2=1. \tag{21}$$

In Fig. 5(a), we show a distribution for $\alpha=0.7$ and $\beta=0.04$, which is $\approx 78\%$ away from the critical value $\beta_*=0.0225$. In this case we can observe a distribution which has asymmetric tails. The negative tail has a sharp cutoff, whereas the positive tail decreases smoothly. Only 0.26% of the second finite-time exponents is positive, indicating that almost all trajectory sections are transversally contracting. This is consistent with the trajectory behavior in the narrow channel that occurs near β_*, but the noteworthy feature here is the relatively small number of positive exponents. Figure 5(b) depicts the same situation, but for $\beta=0.07$, which is about three times the previous deviation away from the critical value. This time the distribution has also a sharp cutoff for negative exponents, while there is a long flat tail of positive exponents (11.4% of their total number). The maximum of the distribution, however, appears not to have moved either toward less negative or positive values of $\lambda_2(10)$, hav-

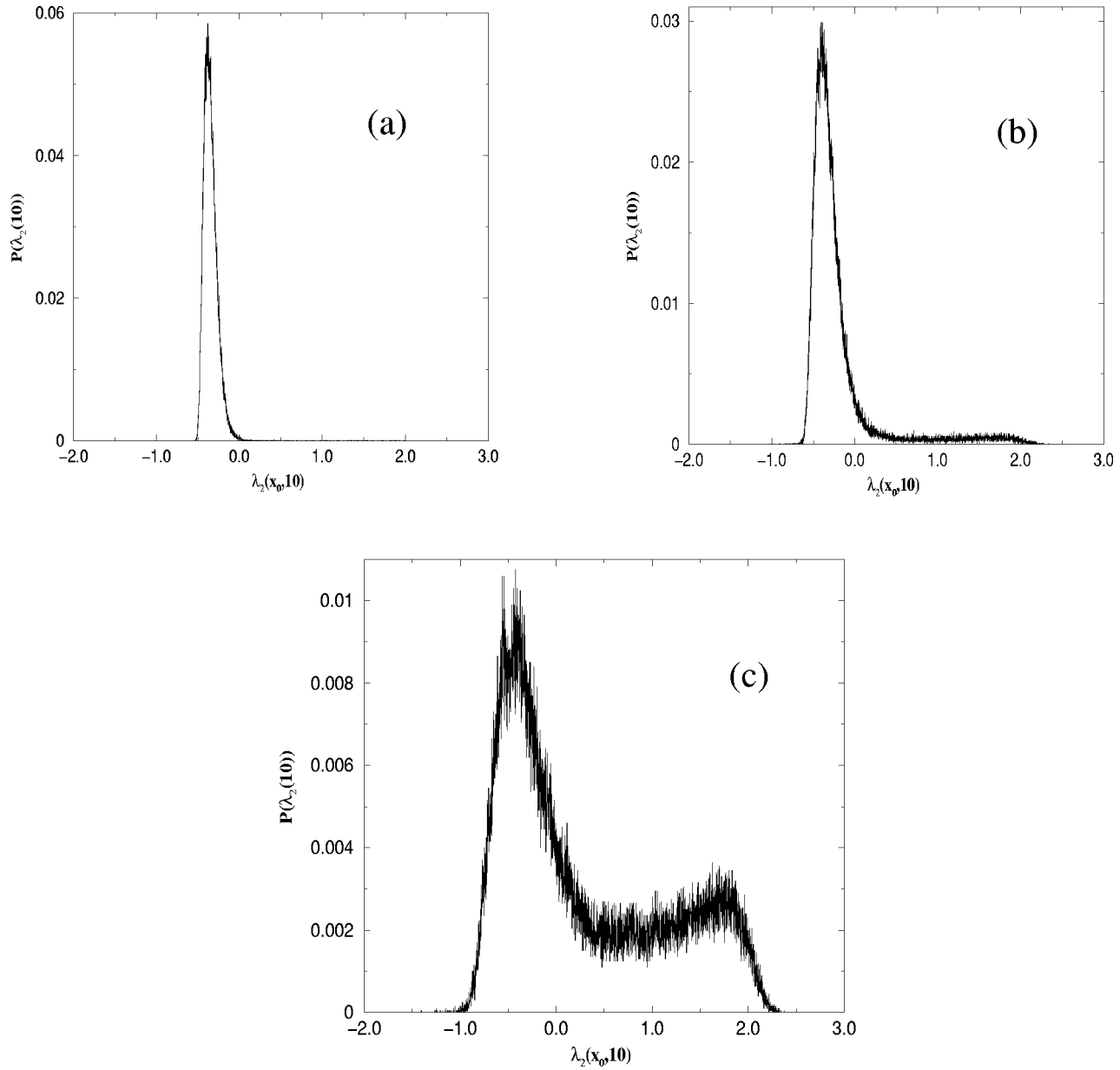

FIG. 5. Probability distribution for the transverse time-10 Lyapunov exponents for $\alpha=0.7$ and (a) $\beta=0.04$, (b) $\beta=0.07$, and (c) $\beta=0.15$.

ing approximately the same value of -0.35 in both cases. The fate of the probability distribution, as we increase further the symmetry-breaking parameter β, is illustrated in Fig. 5(c), where we use $\beta=0.15$. The same general characteristics of Fig. 5(b) are still here, even though we are now very far (almost six times) from the critical value. The negative peak still exists at approximately the same location, but the distribution has broadened in that place. The interesting aspect is the emergence of a second peak in the positive tail. We note that the fraction of positive exponents has increased to 47.3%.

The fraction of positive time-n exponents,

$$f(n)=\int_0^\infty P(\lambda_2(\mathbf{x}_0,n),n)d\lambda_2, \tag{22}$$

has been computed for various values of β, the results being depicted in Fig. 6, showing the correct monotonic increase of this fraction, indicating that for $\beta\approx 0.20$ about half of the exponents are positive. However, this number increases in the map of Eqs. (5) and (6) due to the emergence of the second peak in the positive tail of the distribution. The shape of the curve in Fig. 6 strongly suggests a kind of integrated probability distribution. We have thus computed the cumulative histogram

$$Q(\lambda_2,n)=\int_{-\infty}^{\lambda_2} P(\lambda_2',n)d\lambda_2'=1-\int_{\lambda_2}^{\infty} P(\lambda_2',n)d\lambda_2', \tag{23}$$

where we have used Eq. (21), and $P(\lambda_2)$ is supposed to be Gaussian. In this case $Q(\lambda_2\to-\infty)=0$ and $Q(\lambda_2\to+\infty)=1$. In Fig. 7, we show a cumulative histogram related to the distribution depicted in Fig. 5(c), i.e., for $\beta=0.15$. In fact, if we compare it with the previous figure, qualitatively they are very similar, since for positive exponents it deviates from an

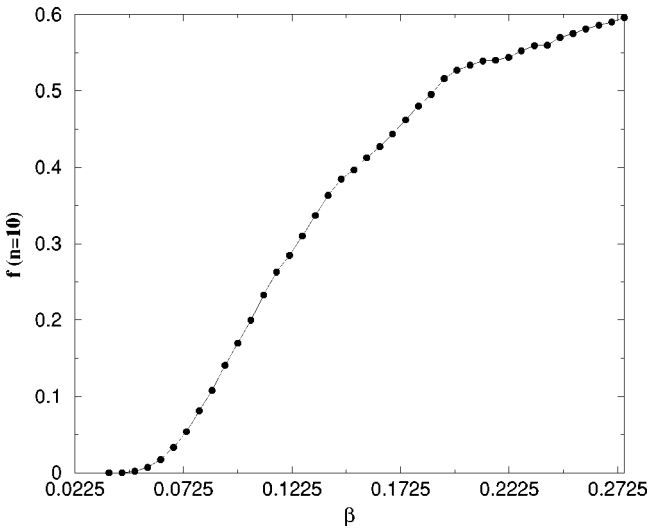

FIG. 6. Fraction of positive transverse time-10 Lyapunov exponents $f(n=10)$ as a function of β, for $\alpha=0.7$ and $\beta_*=0.0225$.

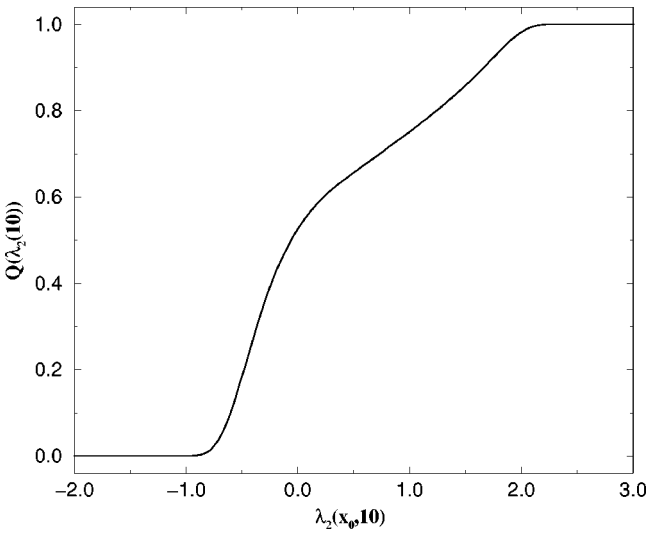

FIG. 7. Cumulative histogram for the transverse time-10 Lyapunov exponents for $\alpha=0.7$ and $\beta=0.15$.

integral of a Gaussian shaped function. Using Eq. (23), it is easy to show that $f(n)=1-Q(0,n)$.

The presence of tails in distributions of finite-time Lyapunov exponents was also reported in a recent paper [16], and it has been found for some dynamical systems exhibiting crisis-induced intermittency, which is a situation very similar to that considered in this paper.

VI. CONCLUSIONS

In summary, this work analyzes the theoretical mechanism for the existence of unstable dimension variability in synchronized coupled chaotic systems. The analysis is corroborated by numerical computations of finite-time Lyapunov exponents.

For invariant sets of a dynamical system, unstable dimension variability can be a strong obstacle to mathematical modeling of physical phenomena, since there is little probability that a real chaotic trajectory is shadowed for moderately long times by a trajectory of a model. This puts some serious doubts on the deterministic model itself, not because it is intrinsically bad, but rather because the dynamics has such a pathology that prevents adequate model shadowability. The consequence is that, although the model is deterministic, we expect to make only relevant statistical predictions, like averages or fluctuations, based on it for reasonable length of times.

ACKNOWLEDGMENTS

This work was made possible by partial financial support from National Science Foundation (Division of International Programs) and CNPq (Conselho Nacional de Desenvolvimento Científico e Tecnológico)—Brazil, through a joint research collaboration project. It was also supported in part by ONR (Physics).

[1] Y.-C. Lai, C. Grebogi, and J. Kurths, Phys. Rev. E **59**, 2907 (1999).
[2] E.J. Kostelich, I. Kan, C. Grebogi, E. Ott, and J.A. Yorke, Physica D **109**, 81 (1997).
[3] R. Abraham and S. Smale, Proc. Symp. Pure Math. (AMS) **14**, 5 (1970).
[4] F.J. Romeiras, C. Grebogi, E. Ott, and W.P. Dayawansa, Physica D **58**, 165 (1992); S.P. Dawson, C. Grebogi, T. Sauer, and J.A. Yorke, Phys. Rev. Lett. **73**, 1927 (1994); S.P. Dawson, *ibid.* **76**, 4348 (1996).
[5] Y.-C. Lai and C. Grebogi, Phys. Rev. Lett. **82**, 4803 (1999).
[6] C. Grebogi, E. Ott, and J.A. Yorke, Phys. Rev. Lett. **50**, 935 (1983).
[7] C. Grebogi, E. Ott, and J.A. Yorke, Ergod. Th. Dynam. Syst. **5**, 341 (1985).
[8] Y.-C. Lai, C. Grebogi, J.A. Yorke, and S.C. Venkataramani, Phys. Rev. Lett. **77**, 55 (1996).
[9] Y.-C. Lai, D. Lerner, K. Williams, and C. Grebogi, Phys. Rev. E **60**, 5445 (1999)..
[10] D.V. Anosov, Proc. Steklov Inst. Math. **90**, 1 (1967); R. Bowen, J. Diff. Eqns. **18**, 333 (1975).
[11] C. Grebogi, S. Hammel, and J.A. Yorke, J. Complexity **3**, 136 (1987); Bull. Am. Math. Soc. **19**, 465 (1988); C. Grebogi, S. Hammel, J.A. Yorke, and T. Sauer, Phys. Rev. Lett. **65**, 1527 (1990); T. Sauer and J.A. Yorke, Nonlinearity **4**, 961 (1991).
[12] L.M. Pecora and T.L. Carroll, Phys. Rev. Lett. **64**, 821 (1990); J.F. Heagy, T.L. Carroll, and L.M. Pecora, *ibid.* **73**, 3528 (1994); **74**, 4185 (1995).
[13] D. Gulick, *Encounters with Chaos* (McGraw-Hill, New York, 1992).
[14] J.L. Kaplan and J.A. Yorke, in *Functional Differential Equations and Approximations of Fixed Points*, Lecture Notes in Mathematics Vol. 730 (Springer-Verlag, New York, 1979), p. 228.
[15] Y. Pomeau and P. Manneville, Commun. Math. Phys. **74**, 189 (1980).
[16] A. Prasad and R. Ramaswany, Phys. Rev. E **60**, 2761 (1999).